

Bqt4 affects relative movement between SPB and nucleolus in fission yeast

Kaiyu Wang¹, Hiroaki Ito¹, Junko Kanoh², and Masaru Ueno^{1, 3*}.

¹Graduate School of Integrated Sciences for Life, Hiroshima University, Hiroshima University, 1-3-1 Kagamiyama, Higashi-Hiroshima 739-8530, Japan

²Department of Life Sciences, Graduate School of Arts and Sciences, The University of Tokyo, 3-8-1 Komaba, Meguro-ku, Tokyo 153-8902, Japan.

³Hiroshima Research Center for Healthy Aging (HiHA), Hiroshima University, Higashi-Hiroshima 739-8530, Japan

*Corresponding author: scmueno@hiroshima-u.ac.jp; Tel: +81-82-424-7768

Abstract

Movement dynamics in the nucleus involve various biological processes, including DNA repair, which is crucial for cancer prevention. Changes in the movement of the components of the nucleus indicate the changes in movement dynamics in the nucleus. In *Schizosaccharomyces pombe*, the inner nuclear membrane protein Bqt4 plays an essential role in attaching telomeres to the nuclear envelope. We observed that the deletion of *bqt4*⁺ caused a significant decrease in the mean square displacement (MSD) calculated from the distance between the nucleolar center and spindle pole body (SPB), hereafter referred to as MSD_(SPB-Nucleolus). The MSD_(SPB-Nucleolus) decrease in *bqt4Δ* was microtubule-dependent. The Rap1-binding ability loss mutant, *bqt4*^{F46A}, and nonspecific DNA-binding ability mutants, *bqt4*^{3E-A}, did not exhibit an MSD_(SPB-Nucleolus) decrease compared to the WT. Moreover, the *bqt4*^{3E-A} *rap1Δ* double mutant and 1-262 amino acids truncated mutant *bqt4ΔN* (263-432), which does not have either Rap1-binding or nonspecific DNA-binding abilities, did not exhibit the MSD_(SPB-Nucleolus) decrease to the same extent as *bqt4Δ*. These results suggest that the unknown function of Bqt4 in the C-terminal domain is essential for the maintenance of the pattern of relative movement between SPB and the nucleolus.

Keywords: Bqt4, nuclear envelope, movement dynamics, mechanical property

Introduction

The term 'movement dynamics in the nucleus' refers to the movement dynamics of structures such as the spindle pole body (SPB), nucleolus, and chromosomes. Movement dynamics in the nucleus involve various biological processes, including DNA repair[1], which is crucial for cancer prevention[2].

Schizosaccharomyces pombe is a widely used model organism. It is a rod-shaped cellular organism with a length of approximately 14 μm and a width of approximately 4 μm . Its spherical nucleus has a diameter of about 2 μm [3]. Within the nucleus, there are only three chromosomes. Because of its simple genome and analyzable nucleus size, *S. pombe* is suitable for nucleus dynamics studies.

In the interphase of *S. pombe*, one of the most apparent internal mechanical forces comes from the microtubules. Microtubules undergo ATP-driven polymerization and depolymerization. The mobilization of the interphase nucleus is purely driven by the force generated through the extension of microtubules contacting interphase microtubule organization centers (iMTOCs) and the SPB[3–5], known as the centrosome in mammals.

The SPB and centromeres are bridged by the Linker of Nucleoskeleton and Cytoskeleton (LINC) complex, forming a microtubule-SPB-LINC-centromere complex[6], by which the force from microtubule polymerization and depolymerization in the cytoplasm can be transmitted to the nucleus and chromosomes[7].

The *S. pombe* nucleus exhibits a distinct movement pattern during interphase. The movement of the nucleus is characterized by a combination of translational and rotational motions, occurring in an oscillatory manner[3]. Under the influence of microtubule forces, the nucleus undergoes deformation, adopting a teardrop shape[8]. This distinctive movement pattern is closely associated with the movement dynamics in the nucleus.

In *S. pombe*, at the opposite side of SPB, the nucleolus wraps around rDNA[9]. The telomere is located at the end of the chromosome and is attached to the nuclear envelope (NE) by the interaction between Rap1 and Bqt4, which are telomere-binding proteins, and the inner nuclear membrane (INM) protein. Bqt4 possesses a nonspecific-dsDNA-binding ability and a Rap1-binding-ability at its N-terminal-domain (NTD)[10,11]. Latest reports show that Bqt4 not only functions as a protein for telomere attachment but also possesses other abilities, such as interacting with the lipid synthesis enzyme Cwh43[12]. Excess Bqt4 induced by ubiquitin-proteasome system (UPS) inhibition causes NE deformation[13]. A study on MtgA, an ortholog of Bqt4 in *Aspergillus nidulans*, implies its function of modulating the nucleus and nucleolus architecture[14]. Based on this information, the non-telomeric function of Bqt4 is strongly suggested.

As mentioned earlier, microtubule dynamics play a key role in movement dynamics in the nucleus. However, how the movement dynamics in the nucleus are maintained by factors other than microtubules requires elucidation.

Relative movement between the SPB and nucleolus can be considered an indicative factor of movement dynamics within the nucleus[15]. In this study, we applied mean

square displacement (MSD) to assess the distance displacement between the SPB and the nucleolus, subsequently referred to as $MSD_{(SPB-Nucleolus)}$, to quantify the relative movement between the SPB and the nucleolus. Our findings indicate that *bqt4*⁺ deletion resulted in a decrease in the $MSD_{(SPB-Nucleolus)}$, and this reduction was not dependent on the function of Bqt4 on NTD. These results suggested the non-telomeric function of Bqt4 on the C-terminal-domain (CTD) in influencing movement dynamics in the nucleus, possibly by altering the transmission of force from microtubules to the nucleolus. The changes in the physical properties of the NE and/or chromosomes caused by *bqt4*⁺ deletion may be the underlying reason for alterations in the transmission of force from microtubules to the nucleolus in the *bqt4Δ* group.

Results

MSD of the distance between nucleolus and SPB decreased in *bqt4Δ* and the different MSD vanishes in the presence of methyl-2-benzimidazole carbamate (MBC)

Previous studies have reported that Bqt4 is an INM protein that can bind with dsDNA nonspecifically and Sad1, Rap1, and Lem2 through its NTD. Deletion of *bqt4*⁺ causes telomere detachment from the NE[10,11]. The detachment of telomere or loss of binding ability to Sad1, Rap1, and Lem2 may alter movement dynamics in the nucleus.

To test this idea, we chose the relative movement between the SPB and the nucleolus as an indicator. We utilized $MSD_{(SPB-Nucleolus)}$ for the quantitative assessment of the relative movement between the SPB and the nucleolus.

For live imaging and tracking, we tagged the SPB and the nucleolus with Sid4-GFP and Gar2-mCherry, respectively, in both the WT and *bqt4Δ* groups for visualization (Supplementary video 1). We calculated the $MSD_{(SPB-Nucleolus)}$ for different time intervals. As the length of time interval increased, the average $MSD_{(SPB-Nucleolus)}$ for individuals plateaued (Fig. S1A-D).

We plotted the average $MSD_{(SPB-Nucleolus)}$ of individuals in different time intervals, hereafter referred to as average $MSD_{(SPB-Nucleolus)}$, in the WT and *bqt4Δ* groups. We observed that the plateau of the average $MSD_{(SPB-Nucleolus)}$ curvature in the WT group is higher than that in the *bqt4Δ* group (Fig. 1A). For further analysis, we selected the points in $\tau = 300s$, which are located at a stable plateau. The height of this point was used to represent the height of the plateau. The plateau height in the *bqt4Δ* group significantly decreased compared to that in the WT group, indicating changes in the movement of the SPB, the nucleolus, or both (Fig. 1B). This kind of reduction was not attributed to the alteration of the growth rate or viability, as *bqt4*⁺ is not an essential gene and viability is unaffected by *bqt4*⁺ deletion (Fig. S1C).

One of the most conspicuous mechanical forces in cells during interphase is the polymerization and depolymerization of microtubules. Because nuclear movement is purely driven by the force originating from microtubule in the cytoplasm during interphase, the relative movement between the SPB and the nucleolus may be driven by microtubules, and the different $MSD_{(SPB-Nucleolus)}$ values in the WT and *bqt4Δ* groups may exhibit microtubule dependency.

Furthermore, if SPB and/or nucleolus movement changes in *bqt4Δ* are caused by the generation of an active (not dependent on microtubules) motion induced by Bqt4 loss, the $MSD_{(SPB-Nucleolus)}$ in the *bqt4Δ* group should differ from that in the WT group with disrupted microtubules. In contrast, if the SPB and/or nucleolus movement changes in the *bqt4Δ* group are caused by changes in their passive (dependent on microtubules) movements induced by Bqt4 loss, the $MSD_{(SPB-Nucleolus)}$ in the *bqt4Δ* group should be same as that in the WT group with disrupted microtubules.

To investigate this possibility, we employed MBC, a microtubule inhibitor[5], to disrupt the microtubules. Based on the image of SPB movement trajectories, the movement area of the SPB in both the WT and *bqt4Δ* groups with MBC is much smaller than that in the absence of MBC (Fig. 1C) (Supplementary Video.1). We examined the height of the $MSD_{(SPB-Nucleolus)}$ curvature plateau in the WT and *bqt4Δ* groups treated with MBC. In contrast to the $MSD_{(SPB-Nucleolus)}$ values of the WT and *bqt4Δ* groups without MBC, the $MSD_{(SPB-Nucleolus)}$ values of the WT and *bqt4Δ* groups with MBC did not exhibit a significant difference, indicating that the different $MSD_{(SPB-Nucleolus)}$ values in the WT and *bqt4Δ* groups are microtubule-dependent (Fig. 1A, B). This data also indicates that the SPB and/or nucleolus movement changes in the *bqt4Δ* group were caused by the changes in their passive movements (movement dependent on microtubules) induced by Bqt4 loss, not by the generation of an active motion (movement independent of microtubules).

Loss of function on NTD of Bqt4 does not decrease $MSD_{(SPB-Nucleolus)}$ to the same extent as *bqt4Δ* null mutant

Because Bqt4 exhibits multifunctionality, we try to elucidate which loss of function of Bqt4 is responsible for $MSD_{(SPB-Nucleolus)}$ decrease. *bqt4^{F46A}* is a Bqt4 mutant that loses its binding ability to proteins with a Bqt4-binding motif (BBM), such as Rap1, Lem2, and Sad1[10]. A loss of the ability to bind with BBM-containing protein may be responsible for the $MSD_{(SPB-Nucleolus)}$ decrease in the *bqt4Δ* group. To verify this hypothesis, we examined $MSD_{(SPB-Nucleolus)}$. The *bqt4^{F46A}* group did not exhibit $MSD_{(SPB-Nucleolus)}$ decrease comparable to that in the *bqt4Δ* group, indicating that the loss of BBM-binding ability is not the cause of the $MSD_{(SPB-Nucleolus)}$ decrease in the *bqt4Δ* group (Fig. 2A).

As Bqt4 can bind to dsDNA non-specifically in vitro, we wondered whether this capability is essential for the maintenance of $MSD_{(SPB-Nucleolus)}$. As the Bqt4 non-specific-dsDNA-binding ability can be severely blocked by *bqt4^{3E-A}*[10], we examined $MSD_{(SPB-Nucleolus)}$ in the *bqt4^{3E-A}* group. No significant difference was observed between the $MSD_{(SPB-Nucleolus)}$ of the WT and *bqt4^{3E-A}* groups (Fig. 2A), indicating that a loss of non-specific dsDNA-binding ability is not responsible for $MSD_{(SPB-Nucleolus)}$ decrease in *bqt4Δ*.

As telomeres are detached from the NE in *bqt4^{F46A}* and *bqt4^{3E-A}*[10], telomere detachment is likely not responsible for $MSD_{(SPB-Nucleolus)}$ decrease. The similar fluorescence intensity of Bqt4^{F46A}, Bqt4^{3E-A}, and Bqt4 suggests comparable protein levels, eliminating the possibility of effects from varying protein levels[10,11].

It is conceivable that Rap1-Bqt4 interaction and the non-specific-dsDNA-binding

ability of Bqt4 function redundantly in terms of SPB–nucleolus relative movement. To investigate this, we deleted *rap1*⁺ in the *bqt4*^{3E-A} background. We observed that although *rap1Δ* exhibited a slight MSD_(SPB-Nucleolus) decrease than in the WT group, in *bqt4*^{3E-A} *rap1Δ*, there was no further decrease. The MSD_(SPB-nucleolus) in *bqt4*^{3E-A} *rap1Δ* was remarkably higher than that in the *bqt4Δ* group (Fig. 2A). This result indicates that a loss of the Rap1-Bqt4 interaction and the non-specific dsDNA-binding ability simultaneously was not sufficient to cause MSD_(SPB-Nucleolus) decrease to the extent observed in *bqt4Δ*.

Proteins with BBM include not only Rap1 but also Lem2 and Sad1. The loss of Rap1 is insufficient to completely mimic the loss of the BBM-binding ability of Bqt4[10]. To exclude the possibility that the BBM-binding ability and non-specific dsDNA-binding ability function redundantly in terms of the SPB–nucleolus relative movement, and exclude the possibility that there is an unknown function on Bqt4-NTD that is responsible for the MSD_(SPB-Nucleolus) decrease in the *bqt4Δ* group, we utilized the Bqt4-NTD truncated mutant *bqt4ΔN(263-432)*, which lacks 1-262 amino acids. *bqt4ΔN(263-432)* expresses comparable protein level as *bqt4FL*, suggested by similar fluorescence intensity [16]. No significant difference in the MSD_(SPB-Nucleolus) between the *bqt4FL* and *bqt4ΔN(263-432)* groups was observed and the higher MSD_(SPB-Nucleolus) in the *bqt4ΔN(263-432)* group than in the *bqt4Δ* group was also observed. These results strongly indicate that NTD function is not responsible for the MSD_(SPB-Nucleolus) decrease in the *bqt4Δ* group (Fig. 2B). An important unknown function of Bqt4-CTD responsible for MSD_(SPB-Nucleolus) decrease was suggested.

Discussion

In this study, in light of the observation that MSD_(SPB-Nucleolus) decreased in the absence of Bqt4, we demonstrated the function of Bqt4 on the regulation of the movement dynamics of SPB and/or the nucleolus.

The deletion of *bqt4*⁺ may decrease the distance between the SPB and the nucleolus which, in turn, causes the reduction of MSD_(SPB-Nucleolus) in the *bqt4Δ* group. However, the distance between the SPB and the nucleolus did not decrease in the *bqt4Δ* group (Fig. S2A). The scatter plot of MSD_(SPB-Nucleolus) and the distance between the SPB and the nucleolus did not exhibit a correlation pattern in either the WT or *bqt4Δ* group (Fig. S2B). Moreover, in the WT and *bqt4Δ* groups, there is a lack of significant correlation coefficients between the MSD_(SPB-Nucleolus) and the distance separating the SPB and the nucleolus in both the WT and *bqt4Δ* groups, indicating the absence of a significant correlation between the mentioned MSD_(SPB-Nucleolus) and distance (Fig. S2C). Consequently, the MSD_(SPB-Nucleolus) decrease in the *bqt4Δ* group was not caused by the reduction of the distance separating the SPB and the nucleolus.

We observed that in the *bqt4*^{F46A} group, the MSD_(SPB-Nucleolus) was slightly higher than that in the WT group, which implies an opposite effect of *bqt4*^{F46A} compared to *bqt4Δ* on the relative movement between the SPB and the nucleolus. A similar phenotype was observed in *lem2Δ* (manuscript in preparation). Lem2 localization on the NE through interactions with Bqt4 and the Lem2-Bqt4 interaction could be impaired by *bqt4*^{F46A}[10,17]. These facts suggest that the MSD increase in the *bqt4*^{F46A} group

1 may be due to the loss of Lem2 on the NE in *bqt4^{F46A}* cells.

2 Interestingly, we observed that MSD_(SPB-Nucleolus) decreased in the *rap1Δ* group,
3 unlike in the *bqt4^{F46A}* or *bqt4^{3E-A}* groups. In three indicated stains, telomeres were
4 detached from the NE[10]. These facts suggest that dysfunctions other than telomere
5 detachment from the NE in the *rap1Δ* group could lead to MSD_(SPB-Nucleolus) decrease.

6 Our study also reveals that the different MSD_(SPB-Nucleolus) values in the WT and
7 *bqt4Δ* groups depend on microtubules, suggesting that changes in SPB and/or nucleolus
8 movements in the *bqt4Δ* group are passive (microtubule-dependent). Hence, the relative
9 movement between the SPB and nucleolus in the *bqt4Δ* group may be altered through
10 changes in the transmission of the microtubule-derived force from the cytoplasm to the
11 nucleus.

12 In the context of microtubule-derived-force transmission, considering the
13 organization of *S. pombe* cells and their nuclei, two potential force mediators would be
14 the NE and chromosomes. There are three to five bundles of microtubules in an
15 interphase cell that make direct contact with the NE through iMTOCs and the SPB[18].
16 This direct contact between the NE and microtubules is required for the NE to serve as
17 a force mediator. Furthermore, several reports show that chromosomes are also
18 remodeled by the force of microtubules[19]. In *S. pombe*, the force from microtubules
19 could be directly transmitted to chromosomes through the SPB-LINC-centromere
20 complex, mobilizing other loci of chromosomes[8]. These facts indicate the mechanical
21 force transmission between chromosomes and microtubules. Chromosomes and the
22 NE are likely simultaneously engaged in a force-mediating role, as it is well-
23 documented that NE deformation and chromosome remolding occur
24 simultaneously[20]. Moreover, apart from centromeres, the rest of the chromosome
25 body is also attached to the NE, such as the telomeres and the mat locus[21]. Interphase
26 microtubules may mobilize the NE and chromosomes attached to the NE
27 simultaneously.

28 Upon obtaining the result indicating that in the *bqt4ΔN* (263-432) group, the
29 MSD_(SPB-Nucleolus) did not exhibit a decrease compared with that in the *bqt4Δ* null
30 mutation group, we suggest the non-telomeric function of Bqt4-CTD on the regulation
31 of relative movement between the SPB and the nucleolus. The non-telomeric function
32 of the CTD of Bqt4 may be responsible for altering microtubule-derived-force
33 transmission by affecting the properties of the NE and chromosomes to decrease
34 MSD_(SPB-Nucleolus). However, it is hard to check whether the loss of CTD of Bqt4 could
35 leads to the decrease in MSD_(SPB-Nucleolus) by using CTD truncated mutant, as the CTD
36 of Bqt4 is responsible for its NE localization[13]. Severe NE rupture and lethality in
37 the *bqt4Δlem2Δ* group suggest the vital role of Bqt4 in membrane integrity maintenance
38 together with Lem2[22]. These facts corroborate the non-telomeric function of Bqt4.
39 Bqt4 is also involved in the regulation of chromatin nature, such as telomere and mat
40 locus tethering, and the maintenance of heterochromatin[21]. Changes in chromatin
41 nature may alter force transmission. In *S. pombe*, the Bqt4 protein level during
42 interphase is approximately 10–30-fold higher than that of the telomere-binding protein
43 Rap1, and its level is similar to that of some membrane function proteins[23,24]. The
44 high protein level of Bqt4 implies a function beyond telomere binding. Further research

is needed to elucidate which of the non-telomeric functions of Bqt4 described above are involved in the maintenance of dynamics in the nuclei.

Materials and Methods

Growth media and live imaging

Cells were grown in YEA (0.5% yeast extract, 3% glucose, and 40 mg/mL adenine, PH was in the range of 6-7) at 30°C. The details for live imaging were described previously[15].

MBC treatment

Cells were cultivated overnight to a density of 1×10^7 cells/mL. MBC was added into the liquid cultivated to 50 µg/ml, the resulting solution was incubated at 30°C for 30 min.

Calculation of MSD_(SPB-Nucleolus)

SPB marker (Sid-GFP and Alp4-tdTomato) and nucleolus marker (Gar2-mCherry and the Gar2-GFP) fluorescence region was tracked by Imaris software (BITPLANE) three-dimensionally (3D). Gar2-mCherry and Gar2-GFP fluorescence region geometric center were used as the 3D position of the nucleolar center. The distance between the SPB and the nucleolar center was determined by calculating the coordinate distance of the SPB and the nucleolar center given by the Imaris software. To quantify the relative SPB-nucleolus movement, the time average MSD (TMSD) of the distance between the SPB and the nucleolus for each cell was used and defined as follows:

$$\text{TMSD}(n, \tau) = \sum_{i=0}^{M-\tau/\Delta t} [d(n, i\Delta t + \tau) - d(n, i\Delta t)]^2 / (M+1 - \tau/\Delta t)$$

Here, $M+1 = T/\Delta t + 1$ is the total number of time points. T is the duration of observation. Δt is the time-interval, $d(n, i\Delta t)$ is the distance of the cell n at time point $i\Delta t$ ($i = 1, 2, 3 \dots M$), and τ ($0, \Delta t, 2\Delta t, 3\Delta t \dots M$) is the lag-time corresponding to the x-axis (Fig. 1A, S1B). The MSD was defined by averaging the TMSD over all cells $\text{MSD}(\tau) = \sum_{n=1}^N \text{TMSD}(n, \tau) / N$, where N is the total cell number. Time-lapse data obtained over 30 min at 30-second intervals with 61 time points were used ($T = 1800$ s, $\Delta t = 30$ s, $M = 60$).

Construction of the gRNA-expressing vector

To delete *bqt4* by CRISPR. The plasmid pAH237[25] was used. The 20 bp gRNA target sequence was designed by finding the PAM nearest to the start codon. Off-target sites were searched using CRISPRdirect and CRISPOR. Two single-strand gRNA oligos were synthesized as follows: gRNA-Fw (5'-caccAATCCCAAAGTGTCGCGCTC-3'), gRNA-Rv (5'-aaacGAGCGCGACACTTTGGGATT3'). Four bases at 5' are plasmid sequences for ligation. 6 µl of 100 µM gRNA-Fw, 6 µl 100 µM gRNA-Rv, 3 µl NEBuffer2.1, and 15 µl DM were mixed, heated at 95°C for 2 min, quenched at room temperature spontaneously for annealing. The resulting dsOligo was diluted 12 times. The plasmid pAH237 was linearized using BbsI at 37°C for 1 h (3 µl 8 ng/µl). The resulting linearized plasmid, diluted dsOligo, and 2 µl ligation high ver2 (Toyobo) were incubated at 16°C for 30 min for ligation. Ligation success was validated by sequencing

1 using primer gRNAseq (5'-TCACGATTATTAAACAGTTTGCT-3') after plasmid
2 amplification. Subsequently, the pAH237 with a gRNA was constructed and referred to
3 as bqt4Δ-pAH237.

4 5 **Preparation of Doner DNA**

6 Doner DNA was designed using TAAA flanked by a 25-bp flanking Cas9 cleavage
7 site and was provided to dsOligo by annealing ssOligo as follows: Oligot (5'-
8 ACACCATTAATCCCAAAGTGTCTGCGTAAaCTCAGGTAATAGAATTTCCTGA
9 TGG-3'), Oligob (5'-
10 CCATCAGGAAATTCTATTACCTGAGtTTACGCGACACTTTGGGATTAATGG
11 TGT-3') with NEBuffer2.1 at 95°C for 2 min, and quenched at room temperature
12 spontaneously.

13 14 **Strain construction**

15 S. pombe strains used in this research are listed in Table S1, the details for strains
16 construction was described in Table S1. The primers and oligos used in this research
17 are listed in Table S2.

18 19 **Funding**

20 MU is supported by MEXT/JSPS KAKENHI, Grant Number 23K05865, and
21 Platform Project for Supporting in Drug Discovery and Life Science Research
22 (Platform for Dynamic Approaches to Living System) from the Ministry of Education,
23 Culture, Sports, Science and Technology (MEXT) and Japan Agency for Medical
24 Research and Development (AMED).

25 26 **Conflicts of interest**

27 No potential conflicts of interest were disclosed.

28 29 **Acknowledgements**

30 We thank Y. Hiraoka, Y. Hirano, Y. Chikashige, T. Toda, M. Yukawa, K. Sawin and
31 the National Bioresource Project Japan for providing the plasmids and strains. We thank
32 H. Senda and K. Ito for technical help, editage(www.editage.jp) for English language
33 editing.

34 35 **Declaration of generative AI and AI-assisted technologies in the writing process**

36 During the preparation of this work the authors used Chat GPT 3.5 in order to
37 improve language and readability, with caution. After using this tool, the authors
38 reviewed and edited the content as needed and takes full responsibility for the content
39 of the publication.

References

- [1] F. Lottersberger, R.A. Karssemeijer, N. Dimitrova, T. De Lange, 53BP1 and the LINC Complex Promote Microtubule-Dependent DSB Mobility and DNA Repair, *Cell* 163 (2015) 880–893. <https://doi.org/10.1016/j.cell.2015.09.057>.
- [2] R. Aleksandrov, R. Hristova, S. Stoyanov, A. Gospodinov, The Chromatin Response to Double-Strand DNA Breaks and Their Repair, *Cells* 9 (2020). <https://doi.org/10.3390/cells9081853>.
- [3] T.H. Hui, F. Zheng, Y. Lin, C. Fu, The linear and rotational motions of the fission yeast nucleus are governed by the stochastic dynamics of spatially distributed microtubules, *J Biomech* 49 (2016) 1034–1041. <https://doi.org/10.1016/j.jbiomech.2016.02.017>.
- [4] R.R. Daga, F. Chang, Dynamic positioning of the fission yeast cell division plane, *Proc Natl Acad Sci U S A* 102 (2005) 8228–8232. <https://doi.org/10.1073/pnas.0409021102>.
- [5] R.R. Daga, K.G. Lee, S. Bratman, S. Salas-Pino, F. Chang, Self-organization of microtubule bundles in anucleate fission yeast cells, *Nat Cell Biol* 8 (2006) 1108–1113. <https://doi.org/10.1038/ncb1480>.
- [6] P.T. Tran, L. Marsh, V. Doye, S. Inoué, F. Chang, A mechanism for nuclear positioning in fission yeast based on microtubule pushing, *Journal of Cell Biology* 153 (2001) 397–411. <https://doi.org/10.1083/jcb.153.2.397>.
- [7] P. Gallardo, R. Barrales, R.R. Daga, S. Salas-pino, Nuclear Mechanics in the Fission Yeast, (2019).
- [8] K.D. Kim, H. Tanizawa, O. Iwasaki, C.J. Corcoran, J.R. Capizzi, J.E. Hayden, K. ichi Noma, Centromeric motion facilitates the mobility of interphase genomic regions in fission yeast, *J Cell Sci* 126 (2013) 5271–5283. <https://doi.org/10.1242/jcs.133678>.
- [9] S. Uzawa, M. Yanagida, Visualization of centromeric and nucleolar DNA in fission yeast by fluorescence in situ hybridization, *J Cell Sci* 101 (1992) 267–275. <https://doi.org/10.1242/jcs.101.2.267>.
- [10] C. Hu, H. Inoue, W. Sun, Y. Takeshita, Y. Huang, Y. Xu, J. Kanoh, Y. Chen, The Inner Nuclear Membrane Protein Bqt4 in Fission Yeast Contains a DNA-Binding Domain Essential for Telomere Association with the Nuclear Envelope, *Structure* 27 (2019) 335–343.e3. <https://doi.org/10.1016/j.str.2018.10.010>.
- [11] C. Hu, H. Inoue, W. Sun, Y. Takeshita, Y. Huang, Y. Xu, J. Kanoh, Y. Chen, Structural insights into chromosome attachment to the nuclear envelope by an inner nuclear membrane protein Bqt4 in fission yeast, *Nucleic Acids Res* 47 (2019) 1573–1584. <https://doi.org/10.1093/nar/gky1186>.
- [12] Y. Hirano, Y. Kinugasa, Y. Kubota, C. Obuse, T. Haraguchi, Y. Hiraoka, Inner nuclear membrane proteins Lem2 and Bqt4 interact with different lipid synthesis enzymes in fission yeast, *J Biochem* 174 (2023) 33–46. <https://doi.org/10.1093/jb/mvad017>.
- [13] T.K. Le, Y. Hirano, H. Asakawa, K. Okamoto, T. Fukagawa, T. Haraguchi, Y. Hiraoka, A ubiquitin–proteasome pathway degrades the inner nuclear membrane protein Bqt4 to maintain nuclear membrane homeostasis, *J Cell Sci* 136 (2023).

1 <https://doi.org/10.1242/jcs.260930>.

2 [14] M. Chemudupati, A.H. Osmani, S.A. Osmani, A mitotic nuclear envelope tether
3 for Gle1 also affects nuclear and nucleolar architecture, *Mol Biol Cell* 27 (2016)
4 3757–3770. <https://doi.org/10.1091/mbc.E16-07-0544>.

5 [15] H. Ito, T. Sugawara, S. Shinkai, S. Mizukawa, A. Kondo, H. Senda, K. Sawai, K.
6 Ito, S. Suzuki, M. Takaine, S. Yoshida, H. Imamura, K. Kitamura, T. Namba, S.
7 ichi Tate, M. Ueno, Spindle pole body movement is affected by glucose and
8 ammonium chloride in fission yeast, *Biochem Biophys Res Commun* 511 (2019)
9 820–825. <https://doi.org/10.1016/j.bbrc.2019.02.128>.

10 [16] Y. Chikashige, M. Yamane, K. Okamasa, C. Tsutsumi, T. Kojidani, M. Sato, T.
11 Haraguchi, Y. Hiraoka, Membrane proteins Bqt3 and -4 anchor telomeres to the
12 nuclear envelope to ensure chromosomal bouquet formation, *Journal of Cell*
13 *Biology* 187 (2009) 413–427. <https://doi.org/10.1083/jcb.200902122>.

14 [17] Y. Hirano, Y. Kinugasa, H. Asakawa, Y. Chikashige, C. Obuse, T. Haraguchi, Y.
15 Hiraoka, Lem2 is retained at the nuclear envelope through its interaction with
16 Bqt4 in fission yeast, *Genes to Cells* 23 (2018) 122–135.
17 <https://doi.org/10.1111/gtc.12557>.

18 [18] S. La Carbona, C. Le Goff, X. Le Goff, Fission yeast cytoskeletons and cell
19 polarity factors: connecting at the cortex, *Biol Cell* 98 (2006) 619–631.
20 <https://doi.org/10.1042/bc20060048>.

21 [19] Y. Maizels, G. Gerlitz, Shaping of interphase chromosomes by the microtubule
22 network, *FEBS Journal* 282 (2015) 3500–3524.
23 <https://doi.org/10.1111/febs.13334>.

24 [20] M. Shokrollahi, K. Mekhail, Interphase microtubules in nuclear organization and
25 genome maintenance, *Trends Cell Biol* 31 (2021) 721–731.
26 <https://doi.org/10.1016/j.tcb.2021.03.014>.

27 [21] H. Ebrahimi, H. Masuda, D. Jain, J.P. Cooper, Distinct ‘safe zones’ at the nuclear
28 envelope ensure robust replication of heterochromatic chromosome regions,
29 *Elife* 7 (2018) 1–32. <https://doi.org/10.7554/eLife.32911>.

30 [22] T. Company, Very-long-chain fatty acid elongase Elo2 rescues lethal defects
31 associated with loss of the nuclear barrier function Yasuha, (2019).

32 [23] A. Carpy, K. Krug, S. Graf, A. Koch, S. Popic, S. Hauf, B. Macek, Absolute
33 proteome and phosphoproteome dynamics during the cell cycle of
34 *Schizosaccharomyces pombe* (fission yeast), *Molecular and Cellular Proteomics*
35 13 (2014) 1925–1936. <https://doi.org/10.1074/mcp.M113.035824>.

36 [24] S. Marguerat, A. Schmidt, S. Codlin, W. Chen, R. Aebersold, J. Bähler,
37 Quantitative analysis of fission yeast transcriptomes and proteomes in
38 proliferating and quiescent cells, *Cell* 151 (2012) 671–683.
39 <https://doi.org/10.1016/j.cell.2012.09.019>.

40 [25] A. Hayashi, K. Tanaka, Short-homology-mediated CRISPR/Cas9-based method
41 for genome editing in fission yeast, *G3: Genes, Genomes, Genetics* 9 (2019)
42 1153–1163. <https://doi.org/10.1534/g3.118.200976>.

43

44

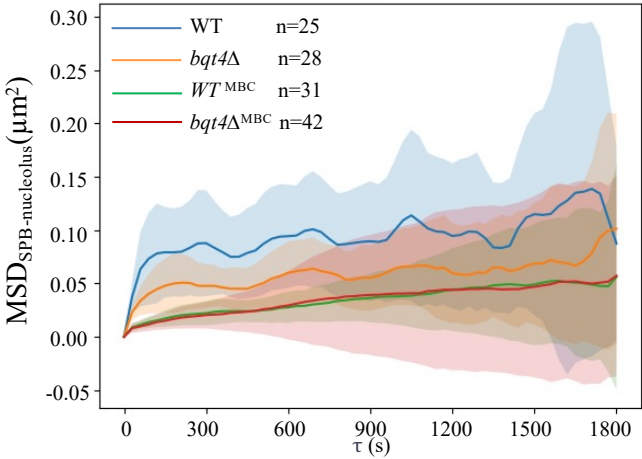
Figure legends

Figure 1. MSD_(SPB-nucleolus) decreased in *bqt4*Δ. Quantification of the relative movement between the SPB(Spindle pole body) and the nucleolus. The mean square displacement (MSD) calculated from the distance between the SPB and the nucleolus is applied to quantify the relative movement between the SPB and the nucleolus. (A) Averaged MSD_(SPB-nucleolus) of WT and *bqt4*Δ strains within different time intervals in YEA, and the group treated with MBC at a concentration of 50 μg/ml for 30 min. (B) The violin and scatter plots of MSD_(SPB-nucleolus) in $\tau = 300$ s in Fig. 1A. Statistical analysis is performed using independent samples t-test and Welch's t-test. p-values '**' for $p < 0.05$; '**' for $p < 0.01$; '***' for $p < 0.001$; '****' for $p < 0.0001$. (C) Image of the cell taken by fluorescence microscopy. Scale bar = 1 μm. Nucleolus is visualized by Gar2-mCherry(red), and SPB and telomeres are visualized individually by Sid4-GFP(green) and lacI-GFP (green) which binds lacO site inserted near *sod2* locus, which is located 80 kb from telomere. The trajectories of SPB and nucleolus movement are indicated by a multicolored gradient line. The images of the third row showed magnifications of boxed regions in the images of the second row.

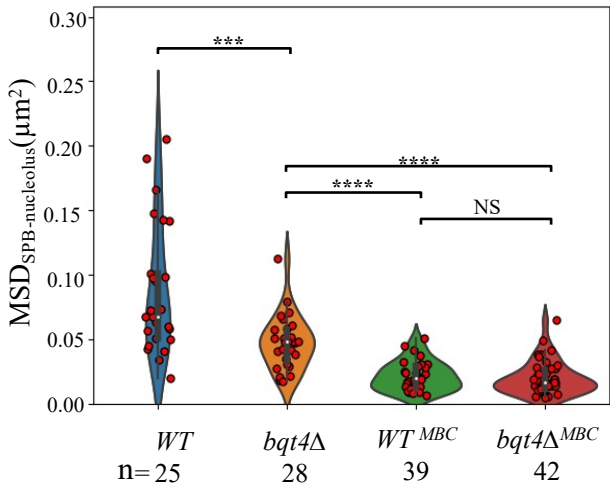
Figure 2. Loss of NTD-function of Bqt4 is not responsible for MSD decrease in *bqt4*Δ. (A) The violin plot and scatter plots of the MSD_(SPB-nucleolus) of the WT, *bqt4*Δ, *bqt4*^{F46A}, *bqt4*^{3E-A}, *rap1*Δ, and *rap1*Δ*bqt4*^{3E-A} strains in $\tau = 300$ s. Sid4-GFP (green) and Gar2-mCherry (red) are used to obtain the position of the SPB and nucleolar center. Statistical analysis is performed using independent samples t-test and Welch's t-test. p-values '**' for $p < 0.05$; '**' for $p < 0.01$; '***' for $p < 0.001$; '****' for $p < 0.0001$. (B) The violin and scatter plots of *bqt4*^{FL}, *bqt4*ΔN(263-432), and *bqt4*Δ strains' MSD_(SPB-nucleolus) in $\tau = 300$ s. Alp4-tdTomato (red) and Gar2-GFP (green) are used to obtain the position of the SPB and nucleolar center. Statistical analysis is performed using independent samples t-test and Welch's t-test. p-values '**' for $p < 0.05$; '**' for $p < 0.01$; '***' for $p < 0.001$; '****' for $p < 0.0001$.

Figure 1

A



B



P-value:
WT vs $bqt4\Delta$: 0.00083
 WT^{MBC} vs $bqt4\Delta$: 1.7007e-07
 $bqt4\Delta$ vs $bqt4\Delta^{MBC}$: 1.9202e-07
 WT^{MBC} vs $bqt4\Delta^{MBC}$: 0.5316

C

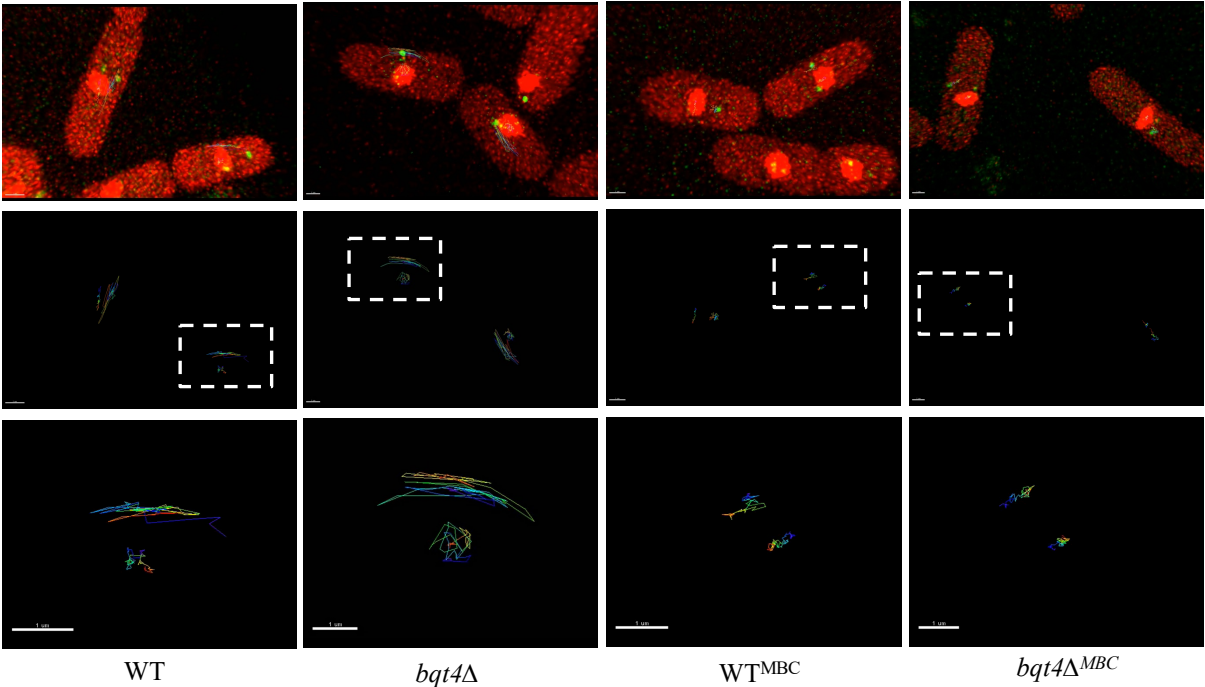
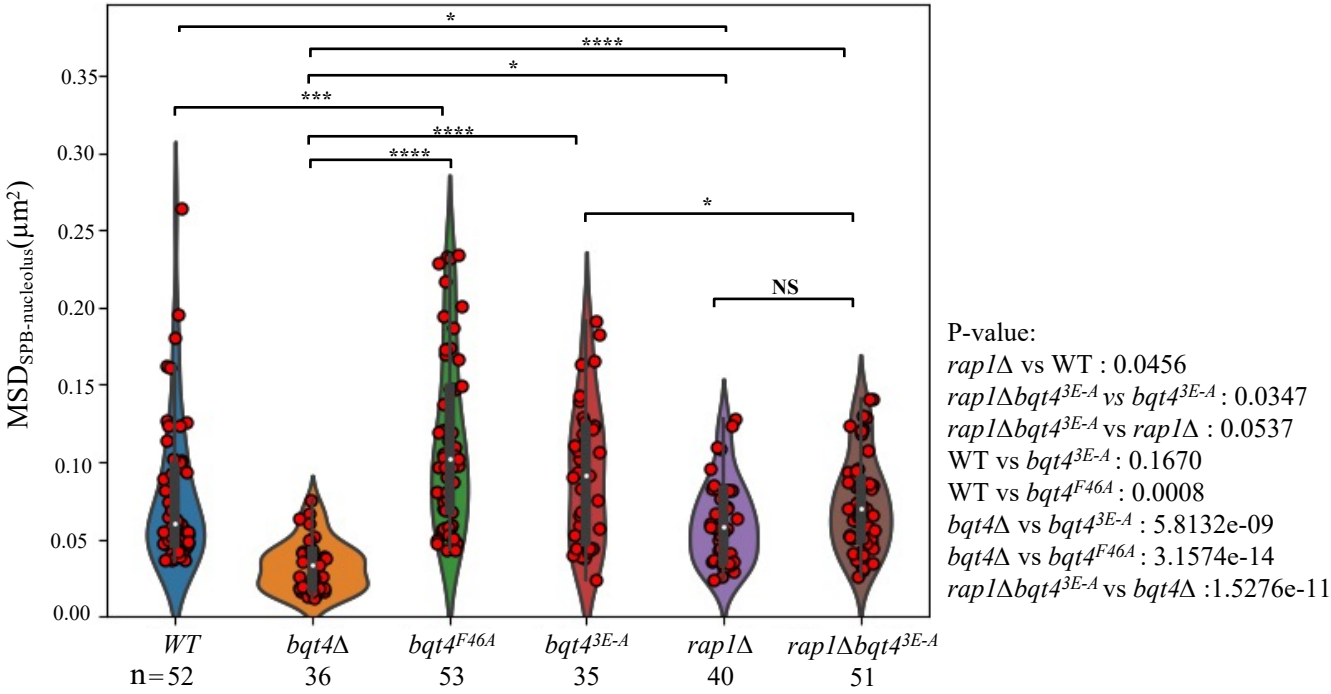
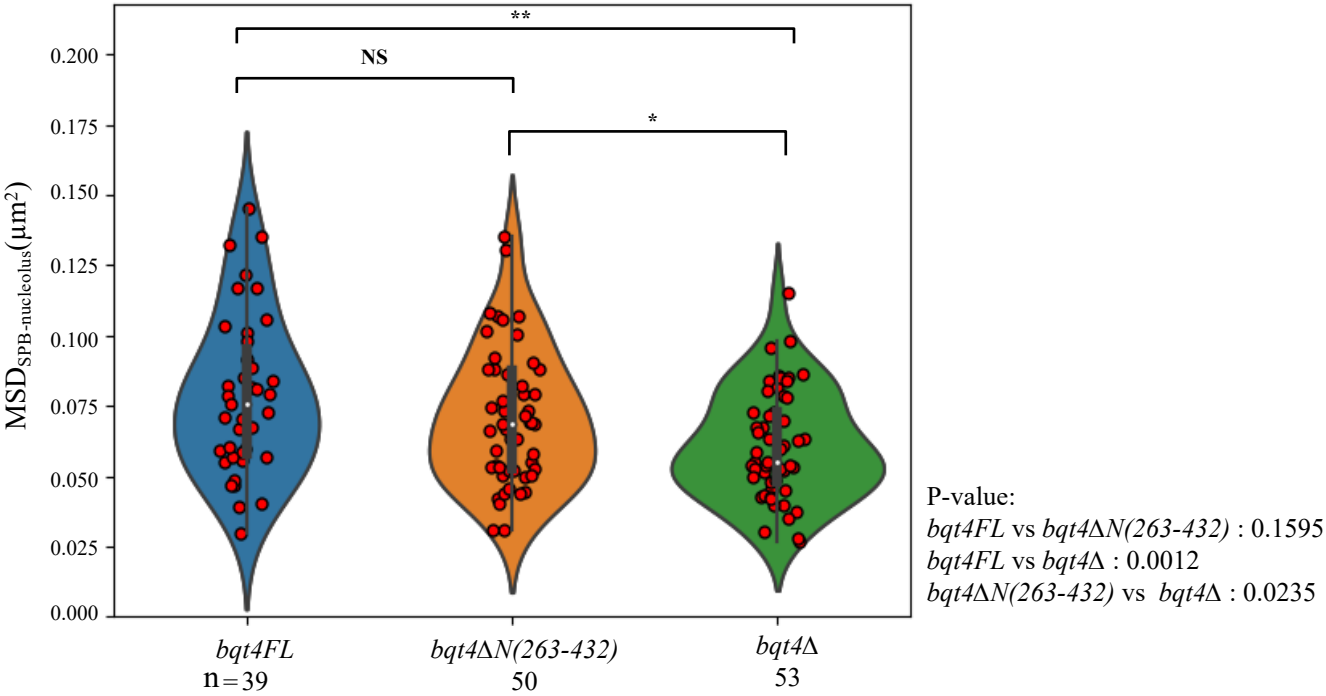


Figure 2

A



B



Supplementary material:

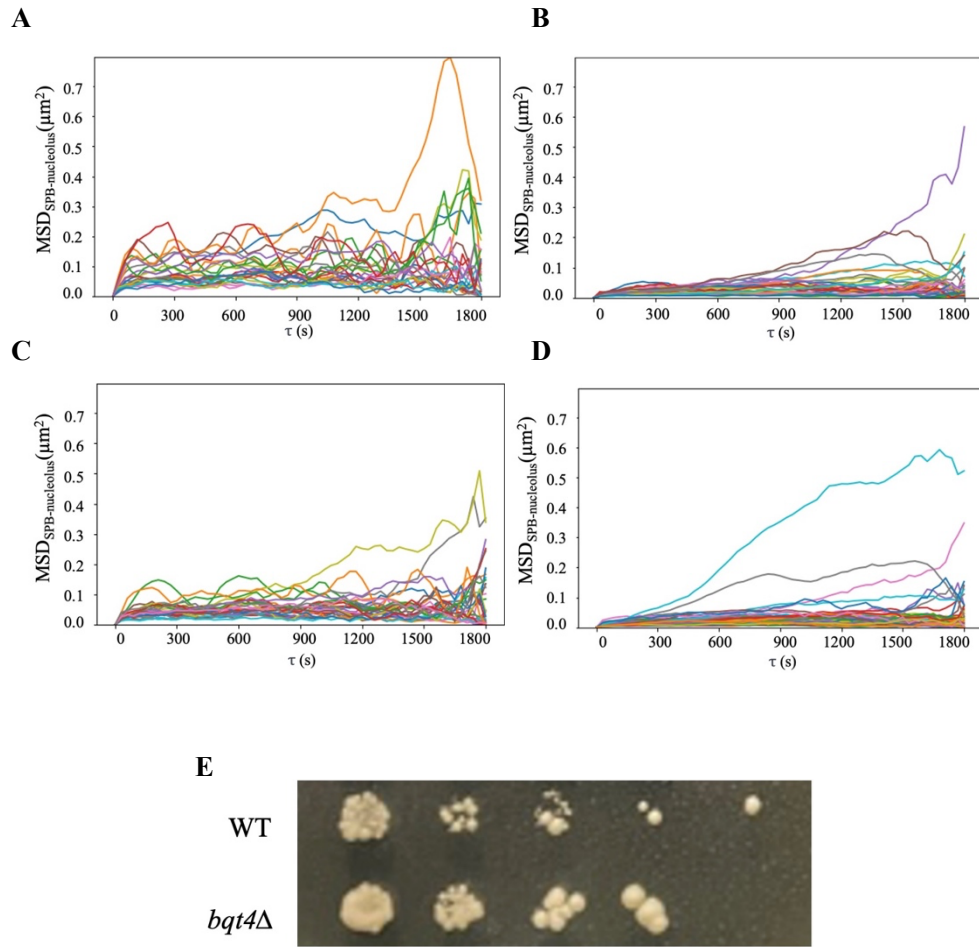


Figure S1. $MSD_{(SPB-nucleolus)}$ is decreased in *bqt4Δ*. (A-D) $MSD_{(SPB-nucleolus)}$ of WT and *bqt4Δ* strains within different time intervals in YEA, and the group treated with MBC at a concentration of 50 $\mu\text{g/ml}$ for 30 min. (E) Spot assay of WT and *bqt4Δ* strains on YEA plate. After incubation at 30 °C in YEA medium, an aliquot of each culture is taken and serially five-fold diluted and spotted onto rich media. Plates are incubated at 30 °C.

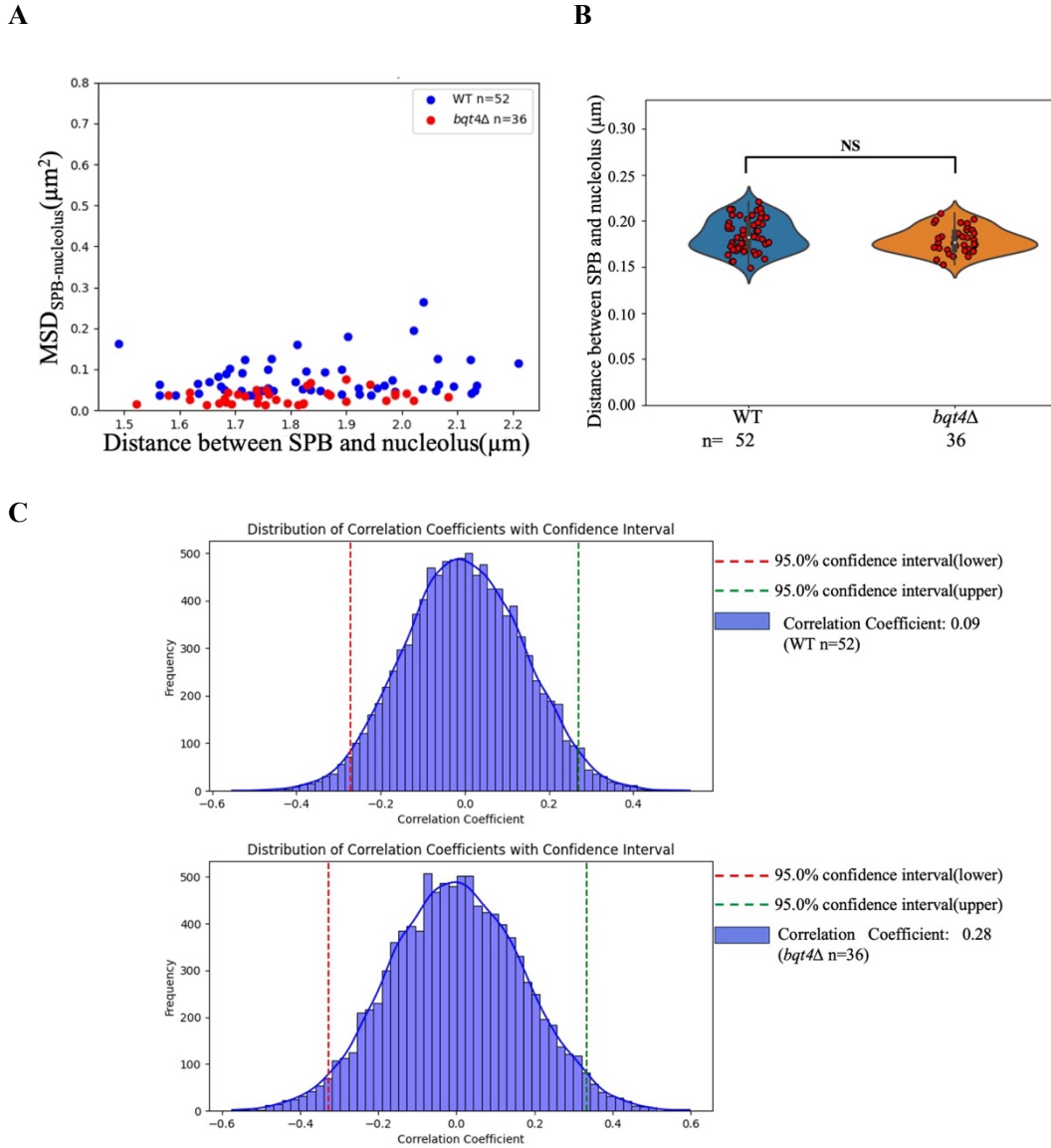


Figure S2. $MSD_{(SPB-nucleolus)}$ decrease in $bqt4\Delta$ is not a result of the decrease in distance between SPB and nucleolus. The $MSD_{(SPB-nucleolus)}$ values of the WT and $bqt4\Delta$ strains in $\tau = 300$ s shown in Fig 2A were used for the analysis. The WT and $bqt4\Delta$ strain distance is the average of the distance between the SPB and the nucleolus in 61 time points in individual cells. (A) Violin and scatter plots of distance in WT and $bqt4\Delta$ strains. Statistical analysis is performed using independent samples t-test. P-value between WT and $bqt4\Delta$ group is 0.1177.

(B) Scatter plot of distance and MSD in WT and $bqt4\Delta$ strains. (C) Distribution of correlation coefficient (Spearman) of $MSD_{(SPB-nucleolus)}$ and distance in WT and $bqt4\Delta$. The 95% confidence interval, which was obtained using the bootstrap method (bootstrap sample number = 10000), is shown between red and green dashed lines. In both WT and $bqt4\Delta$ strains, correlation coefficient = 0 is included in 95% confidence interval, which suggests a lack of significant correlation.

Supplementary video Legend

Supplementary video 1. Video of the WT, *bqt4Δ*, WT treated with MBC, *bqt4Δ* treated with MBC groups taken by fluorescence microscopy. The nucleolus is tagged by mCherry (red), and SPB and telomeres are tagged by GFP (green). The trajectories of SPB and nucleolar movement are shown by a multicolored gradient line. The time interval for each picture is 30 s, frames = 10.

Table S1. *S. pombe* strains used in this study.

Strain	Strain genotype	Source
43-D08	<i>h+ bqt4Δ::kanMX4 ade6-M210 ura4-D18 leu1-32</i>	Lab stock
13-G10	<i>h⁺ ade6-210 leu1 lys1 ura4 sod2.prox::kanr-ura4⁺-lacOp his7⁺::lacI-GFP sid4::sid4⁺-GFP-natMX6 gar2::gar2⁺-mCherry-hphMX6 orfΔ(bqt4Δ)::bsd</i>	Lab stock
1-1-1	<i>1-1-1:h⁺ade6-210 leu1 lys1 ura4 sod2.prox::kanr-ura4⁺-lacOp his7⁺::lacI-GFP Sid4-GFP-nat Gar2-mCherry-hph.</i>	H.Ito [1]
102-D10	<i>h⁺ ade6-210 leu1 lys1 ura4 sod2.prox::kanr-ura4⁺-lacOp his7⁺::lacI-GFP Sid4-GFP-nat Gar2-mCherry-hph bqt4Δ::bsd</i>	Lab stock
JP4606	<i>h90 ade6-M210 leu1-32 ura4-D18 bqt4^{F46A}</i>	J. Kanoh [2]
98-F08	<i>h90 ade6-M210 leu1-32 ura4-D18 bqt4^{F46A} sid4-GFP-natR</i>	This study
101-C04	<i>h90 ade6-M210 leu1-32 ura4-D18 bqt4^{F46A} sid4-GFP-natR Gar2-mCherry-hph</i>	This study
JP4823	<i>h90 ade6-M210 leu1-32 ura4-D18 bqt4^{3E-A}</i>	J. Kanoh [2]
101-D03	<i>h90 ade6-M210 leu1-32 ura4-D18 bqt4^{3E-A} sid4-GFP-nat</i>	This study
104-A09	<i>h90 ade6-M210 leu1-32 ura4-D18 bqt4^{3E-A} sid4-GFP-nat Gar2-mCherry-hph</i>	This study
FY14174 JK805	<i>h90 ade6-M210 leu1-32 ura4-D18 rif1:12Myc:ura4⁺ rap1::kanR</i>	NBRP
78-A02	<i>h⁺ ade6-210 leu1 lys1 ura4 sod2.prox::bsdMX6-ura4⁺-lacOp his7⁺::lacI-GFP sid4::sid4⁺-GFP-natMX6 gar2::gar2⁺-mCherry-hphMX6</i>	P. Emami [3]
78-E01	<i>h⁺ ade6-210 leu1 lys1 ura4 sod2.prox::bsdMX6-ura4⁺-lacOp his7⁺::lacI-GFP sid4::sid4⁺-GFP-natMX6 gar2::gar2⁺-mCherry-hphMX6 rap1::kanR</i>	This study

104-D08	<i>h90 ade6-M210 leu1-32 ura4-D18 bqt4^{3E-A} sid4-GFP-nat, rap1::kanR</i>	This study
104-I01	<i>h90 ade6-M210 leu1-32 ura4-D18 bqt4^{3E-A}, sid4-GFP-nat, rap1::kanR, Gar2-mcherry-hph</i>	This study.
CRLt79	<i>hm, lys1+::GFP-bqt4,ura48,ade6-210,bqt4D::ura4+</i>	Y. Hiraoka [4]
107-G04	<i>hm, lys1+::GFP-bqt4,ura4-D18,ade6-210,bqt4D::ura4+ alp4- tdTomato-natR</i>	This study
108-E10	<i>hm, lys1+::GFP-bqt4,ura4-D18,ade6-210,bqt4D::ura4+ alp4-tdTomato-natR GAR2-GFP::kanMX6</i>	This study
CRLs25	<i>h90, leu1-32, lys1+::GFP-bqt4-dN,ura4-D18,ade6-210 bqt4D::ura4+,taz1-mCherry::kanR</i>	Y. Hiraoka [4]
104-B09	<i>h90, leu1-32, lys1+::GFP-bqt4-dN,ura4-D18,ade6-210 bqt4D::ura4+,taz1-mCherry::bsd</i>	This study
104-E02	<i>h90, leu1-32, lys1+::GFP-bqt4-dN,ura4-D18,ade6-210 bqt4D::ura4+,taz1-mCherry::bsd GAR2-GFP::kanMX6</i>	This study
104-J09	<i>h90, leu1-32, lys1+::GFP-bqt4-dN,ura4-D18,ade6-210 bqt4D::ura4+,taz1-mCherry::bsd GAR2-GFP::kanMX6,Alp4- tdTomato-natR</i>	This study
iHR2085	<i>h+alp4-tdTomato-natR leu1 ura4 his2</i>	K. Sawin [5]
13-B09/sw240	<i>h- leu1-32 ura4-D18 GAR2-GFP::kanMX6</i>	Lab stock
115-j03	<i>h+alp4-tdTomato-natR leu1 ura4 his2 bqt4Δ</i>	This study
116-E08	<i>h+alp4-tdTomato-natR leu1 ura4 his2 bqt4Δ GAR2-GFP::kanMX6</i>	This study

Details of strains construction

Construction of 102-D10

The *bsd* marker gene fragment was amplified from pBSDZA12-mCherry-atb⁺, which is Bsd-replaced-pNATZA12-mCherry-atb2⁺[3] with the primers Mxt (5'-gacatggaggcccaataac-3') and Mxb (5'-tggatggcggcgtagtagt-3'), was introduced into strain 43-D08 (*h⁺ bqt4Δ::kanMX4 ade6-M210 ura4-D18 leu1-32*). The resulting strain 13-G10 genotype is *h⁺ bqt4::bsd ade6-M210 ura4-D18 leu1-32*. The PCR product fragments obtained from PCR in which 13-G10(*h⁺ bqt4::bsd ade6-M210 ura4-D18 leu1-32*) was used as the template, bqt4t: (5'-CGTAGATAGCTGCATCAGCG-3') and bqt4b2: (5'-ttgtcctcaaccttgaatatag-3'), were individually used as the top and bottom primers, respectively, and was transformed into 1-1-1 (*h⁺ ade6-210 leu1 lys1 ura4 sod2.prox::kanr-ura4⁺-lacOp his7⁺::lacI-GFP sid4::sid4⁺-GFP-natMX6 gar2::gar2⁺-mCherry-hphMX6*). Then, strain 102-D10:(*h+ade6-210 leu1 lys1 ura4 sod2.prox::kanr-ura4⁺-lacOp his7⁺::lacI-GFP Sid4-GFP-nat Gar2-mCherry-hph bqt4Δ::bsd*) was constructed.

Construction of 101-C04

The Sid4-GFP-nat plasmid and Gar2-mCherry-hph plasmid[1] were individually linearized using StuI and AflII and transformed into JP4606 (*h90 ade6-M210 leu1-32 ura4-D18 bqt4^{F46A}*). 98-F08 (*h90 ade6-M210 leu1-32 ura4-D18 bqt4^{F46A} sid4-GFP-natR*) and 101-C04 (*h90 ade6-M210 leu1-32 ura4-D18 bqt4^{F46A} sid4-GFP-natR Gar2-mCherry-hph*) were constructed subsequently.

Construction of 104-A09

The Sid4-GFP-nat plasmid and Gar2-mCherry-hph plasmid[1] were individually linearized using StuI and AflII and transformed into JP4823 (*h90 ade6-M210 leu1-32 ura4-D18 bqt4^{3E-A}*). Strains 101-D03: (*h90 ade6-M210 leu1-32 ura4-D18 bqt4^{3E-A} sid4-GFP-nat*) and 104-A09 (*h90 ade6-M210 leu1-32 ura4-D18 bqt4^{3E-A} sid4-GFP-nat Gar2-mCherry-hph*) were constructed subsequently.

Construction of 78-E01

The PCR products obtained by PCR in which 10-D02 (*h90 ade6-M210 leu1-32 ura4-D18 rif1:12Myc:ura4⁺ rap1:kanR*) was used as the template, rap1 top(5'-cgttttggctaggtctttcat-3') and rap1 bot (5'-atattatgctagtcaaccct-3'), were individually used as the top and bottom primers, respectively, and transformed into strain 78-A02 (*h⁺ ade6-210 leu1 lys1 ura4 sod2.prox::bsdMX6-ura4⁺-lacOp his7⁺::lacI-GFP sid4::sid4⁺-GFP-natMX6 gar2::gar2⁺-mCherry-hphMX6*) to construct 78-E01 (*h⁺ ade6-210 leu1 lys1 ura4 sod2.prox::bsdMX6-ura4⁺-lacOp his7⁺::lacI-GFP sid4::sid4⁺-GFP-natMX6 gar2::gar2⁺-mCherry-hphMX6 rap1:kanR*).

Construction of 104-I01

The PCR products obtained by PCR in which the 78-E01 (*h⁺ ade6-210 leu1 lys1 ura4 sod2.prox::bsdMX6-ura4⁺-lacOp his7⁺::lacI-GFP sid4::sid4⁺-GFP-natMX6 gar2::gar2⁺-mCherry-hphMX6 rap1::kanR*) genome was used as the template, rap1 top (5'-cgtttttggttagtctttcat-3') and rap1 bot (5'-atattatgctagtcaccct-3') were individually used as the top and bottom primers, respectively, and transformed into 101-D03: (*h90 ade6-M210 leu1-32 ura4-D18 bqt4^{3E-A} sid4-GFP-nat*) to construct 104-D08: (*h90 ade6-M210 leu1-32 ura4-D18 bqt4^{3E-A} sid4-GFP-nat, rap1::kanR*). The resulting strain underwent transformation again to introduce the linearized-Gar2-mCherry-hph plasmid using AflII. Subsequently, strain 104-I01: (*h90 ade6-M210 leu1-32 ura4-D18 bqt4^{3E-A}, sid4-GFP-nat, rap1::kanR, Gar2-mcherry-hph*) was constructed.

Construction of 104-J09

The *bsd* maker gene fragment amplified from pBSDZA12-mCherry-atb⁺ with the primers Mxt (5'-gacatggaggccagaatac-3') and Mxb (5'-tggatggcggcgtagtgc-3') was introduced into strain CRLs25 (*h90, leu1-32, lys1+::GFP-bqt4-dN, ura4-D18, ade6-210 bqt4D::ura4+, taz1-mCherry::kanR*), and the resulting strain was 104-B09 (*h90, leu1-32, lys1+::GFP-bqt4-dN, ura4-D18, ade6-210 bqt4D::ura4+, taz1-mCherry::bsd*) of which KanR was replaced by Bsd. The DNA fragments obtained from PCR in which 13-B09 (*h- leu1-32 ura4-D18 GAR2-GFP::kanMX6*) was used as the template, Gar2top: (5'-Ctcaacaacgtgcggg-3') and Gar2bb (5'-GTGATCAACGATGATTGTGag-3'), were individually used as the top and bottom primers, respectively, and transformed into 104-B09 (*h90, leu1-32, lys1+::GFP-bqt4-dN, ura4-D18, ade6-210 bqt4D::ura4+, taz1-mCherry::bsd*). Subsequently, the resulting strain 104-E02 (*h90, leu1-32, lys1+::GFP-bqt4-dN, ura4-D18, ade6-210 bqt4D::ura4+, taz1-mCherry::bsd GAR2-GFP::kanMX6*) was inserted using the DNA fragments obtained from PCR in which iHR2085 (*h+alp4-tdTomato-natR leu1 ura4 his2*) was used as the template, Alp4top: (5'-AGAATAGTGCTTGGCGTCTC-3') and Alpt4bot (5'-ATTCCTCAGGCATTATCAGC-3'), were used as the top and bottom primers, respectively, to construct 104-J09 (*h90, leu1-32, lys1+::GFP-bqt4-dN, ura4-D18, ade6-210 bqt4D::ura4+, taz1-mCherry::bsd GAR2-GFP::kanMX6, Alp4-tdTomato-natR*). Strains undergoing transformation were selected according to sequencing results, and the primer sets that were used for sequencing were Gar2: Gar2tcheck (5'-Ggtcgtatggtcaacttag-3'), Gar2bb (5'-GTGATCAACGATGATTGTGag-3'), Alp4: Alp4t4 (5'-TCCCGCAAAGCTATTATTCG-3'), and Alpt4bot (5'-ATTCCTCAGGCATTATCAGC-3').

Construction of 108-E10

The DNA fragments obtained from PCR in which iHR2085 (*h+alp4-tdTomato-natR leu1 ura4 his2*) was used as the template, Alp4top: (5'-AGAATAGTGCTTGGCGTCTC-3') and Alpt4bot (5'-ATTCCTCAGGCATTATCAGC-3'), were individually used as the top and bottom primers, respectively, and transformed into CRLt79 (*hm, lys1+::GFP-bqt4, ura48, ade6-210, bqt4D::ura4+*) to construct 107-G04 (*hm, lys1+::GFP-bqt4, ura4-D18, ade6-210, bqt4D::ura4+ alp4-tdTomato-natR*). The DNA fragments obtained from

PCR in which 13-B09 (*h-leu1-32 ura4-D18 GAR2-GFP::kanMX6*) was used as the template, Gar2top: (5'-Ctcaacaacgtgcggg-3') and Gar2bb (5'-GTGATCAACGATGATTGTGag-3'), were individually used as the top and bottom primers, respectively, and transformed into 107-G04 (*hm,lys1+::GFP-bqt4,ura4-D18,ade6-210,bqt4D::ura4+ alp4-tdTomato-natR*), and strain 108-E10 (*hm,lys1+::GFP-bqt4,ura4-D18,ade6-210,bqt4D::ura4+ alp4-tdTomato-natR GAR2-GFP::kanMX6*) was constructed. Strains undergoing transformation were selected according to sequencing results, and the primer sets that were used for sequencing were Gar2: Gar2tcheck (5'-Ggtcgtatggtcaacttag-3'), Gar2bb (5'-GTGATCAACGATGATTGTGag-3'), Alp4: Alp4t4(5'-TCCCGCAAAGCTATTATTCG-3'), and Alp4t4bot (5'-ATTCCTCAGGCATTATCAGC-3')

Construction of 116-E08

To delete *bqt4*⁺, the plasmid *bqt4Δ*-pAH237 and the dsDoner DNA were transformed into iHR2085 (*h+alp4-tdTomato-natR leu1 ura4 his2*) using a transformation kit (*S. pombe* Direct Transformation Kit, Wako Japan). After popping out the plasmid and sequencing with the primer *bqt4deletioncheck*t (5'GCACCACTATTGCTCTATAC-3'), the successes of the construction of 115-j03 (*h+alp4-tdTomato-natR leu1 ura4 his2 bqt4Δ*) was validated, the DNA and amino acid sequences are showed as follows, '*' for stop codon:

DNA sequence

WT	5' AAAGTGTCGCG----CTCAGGTAATAGAA 3'	(from No.166bp)
<i>bqt4Δ</i>	5' AAAGTGTCGCGTAAACTCAGGTAATAGAA 3'	(from No.166bp)

Amino acid sequence

WT	N- MTENEKSRSLPAERNPLYKDDTLDH	from No.1 amino acid
<i>bqt4Δ</i>	N- MTENEKSRSLPAERFVYLKKTN*Y*	from No.1 amino acid

The TAAA insertion was located at 177 bp and caused a frame shift. Consequently, the amino acid sequence changed from No. 15 and a stop codon was generated at No. 24. The DNA fragments obtained from PCR in which 13-B09 (*h-leu1-32 ura4-D18 GAR2-GFP::kanMX6*) was used as the template, Gar2top: (5'-Ctcaacaacgtgcggg-3') and Gar2bb (5'-GTGATCAACGATGATTGTGag-3') were individually used as the top and bottom primers, respectively, and transformed into the resulting strain. Subsequently, 116-E08 (*h+alp4-tdTomato-natR leu1 ura4 his2 bqt4Δ GAR2-GFP::kanMX6*) was constructed. The strain undergoing transformation was selected according to the sequencing results. The primer sets that were used for sequencing were Gar2: Gar2tcheck (5'-Ggtcgtatggtcaacttag-3') and Gar2bb (5'-GTGATCAACGATGATTGTGag-3').

Table S2. primer and Doner DNA ss oligo used in this study.

name	Sequence (from 5' to 3')
gRNA-Fw	caccAATCCCAAAGTGTCGCGCTC
gRNA-Rv	aaacGAGCGCGACACTTTGGGATT
gRNAseq	TCACGATTATTAAACAGTTTGCT
Doner DNA oligot	ACACCATTAATCCCAAAGTGTCGCGTAAaCTCAG GTAATAGAATTTCTGATGG
Doner DNA oligob	CCATCAGGAAATTCTATTACCTGAGtTTACGCGA CACTTTGGGATTAATGGTGT
Mxt	gacatggaggcccagaatac
Mxb	tggatggcgcggttagtatac
bqt4t	CGTAGATAGCTGCATCAGCG
Bqt4b	ttgtcctcaacctgaatatac
rap1 top	cgtttttggctaggtctttcat
rap1 bot	atattatgctagtcaaccct
Gar2top	Ctcaacaacgtgcggg
Gar2bb	GTGATCAACGATGATTGTGag
Alp4top	AGAATAGTGCTTGGCGTCTC
Alpt4bot	ATTCCTCAGGCATTATCAGC
Gar2tcheck	Ggtcgtaggtcaacttag
Alp4t4	TCCCGCAAAGCTATTATTCG
bqt4deletion checkt	GCACCACTATTGCTCTATAC

References:

- [1] H. Ito, T. Sugawara, S. Shinkai, S. Mizukawa, A. Kondo, H. Senda, K. Sawai, K. Ito, S. Suzuki, M. Takaine, S. Yoshida, H. Imamura, K. Kitamura, T. Namba, S. ichi Tate, M. Ueno, Spindle pole body movement is affected by glucose and ammonium chloride in fission yeast, *Biochem Biophys Res Commun* 511 (2019) 820–825. <https://doi.org/10.1016/j.bbrc.2019.02.128>.
- [2] C. Hu, H. Inoue, W. Sun, Y. Takeshita, Y. Huang, Y. Xu, J. Kanoh, Y. Chen, Structural insights into chromosome attachment to the nuclear envelope by an inner nuclear membrane protein Bqt4 in fission yeast, *Nucleic Acids Res* 47 (2019) 1573–1584. <https://doi.org/10.1093/nar/gky1186>.
- [3] P. Emami, M. Ueno, 3,3'-Diindolylmethane induces apoptosis and autophagy in fission yeast, *PLoS One* 16 (2021) 1–20. <https://doi.org/10.1371/journal.pone.0255758>.
- [4] Y. Chikashige, M. Yamane, K. Okamasa, C. Tsutsumi, T. Kojidani, M. Sato, T. Haraguchi, Y. Hiraoka, Membrane proteins Bqt3 and -4 anchor telomeres to the nuclear envelope to ensure chromosomal bouquet formation, *Journal of Cell Biology* 187 (2009) 413–427. <https://doi.org/10.1083/jcb.200902122>.
- [5] I. Samejima, V.J. Miller, L.M. Groocock, K.E. Sawin, Two distinct regions of Mto1 are required for normal microtubule nucleation and efficient association with the γ -tubulin complex in vivo, *J Cell Sci* 121 (2008) 3971–3980. <https://doi.org/10.1242/jcs.038414>.